ELSEVIER

Journal of Nuclear Materials 255 (1998) 234–242

journal of nuclear materials

The influence of nitrogen dioxide on the oxidation of UO_2 in air at temperatures below 275°C

Roderick J. McEachern *, Sham Sunder [1], Peter Taylor, Diane C. Doern, Neil H. Miller, Donald D. Wood

Research Chemistry Branch, Atomic Energy of Canada, Whiteshell Laboratories, Pinawa, Manitoba, Canada R0E 1L0

Received 18 September 1997; accepted 20 January 1998

Abstract

Specimens of polycrystalline, sintered UO_2 were cut from unirradiated CANDU fuel, and heated in air or air + NO_2 mixtures (up to 1 vol.% NO_2), to investigate the effects of nitrogen oxides on the rates of oxidation to U_3O_7 and U_3O_8. Oxidized specimens were analyzed by X-ray diffraction (XRD) and X-ray photoelectron spectroscopy to determine the extent of surface oxidation. The kinetic expression for the formation of U_3O_7 was initially parabolic, but switched to linear at long reaction times. The first, parabolic stage of oxidation to U_3O_7 was accelerated slightly by the addition of small quantities of NO_2 to air, probably because NO_2 increases the oxygen potential of the outermost surface of the UO_2 by forming a thin film of UO_3. The rate of oxidation in the region of linear kinetics is approximately the same for all atmospheres up to 1.0% NO_2. The effect of NO_2 on the rate of U_3O_8 formation is difficult to ascertain because of the close similarity between the XRD patterns of α-UO_3 and U_3O_8. However, it appears that there is a substantial increase in the rate of formation of higher oxides (U_3O_8 and possibly also UO_3) in the presence of NO_2. These results indicate that the effect of nitrogen oxides (which are formed by radiolysis of air) should be included in detailed models of air oxidation of irradiated fuel.

1. Introduction

The oxidation of UO_2 to U_3O_8 has been investigated intensively for over 40 years ([1], and references therein). One reason for this sustained interest is that the 36% volume increase, associated with the conversion of UO_2 to U_3O_8, can cause swelling and splitting of defective fuel elements stored in air at elevated temperatures [2–4]. Therefore, it is important to understand the kinetics of U_3O_8 formation on irradiated UO_2 fuel under dry storage conditions.

Small amounts of nitrogen oxides are known to influence the kinetics of air oxidation of UO_2. This may be relevant to dry storage of irradiated UO_2 fuel, because NO_x compounds can be formed by the radiolysis of air in a storage vessel; in the presence of moisture, nitric acid is also formed. Accelerated oxidation of UO_2 powder by NO_2–O_2 mixtures, as compared with pure oxygen, was first reported over 40 years ago [5]. More recently, researchers at Pacific Northwest Laboratories found that the addition of 1% NO_2 to air accelerates the oxidation of unirradiated UO_2 pellets at 215 to 250°C [6–8]; however, variations in sample densities prevented quantitative interpretation of this work.

In addition to accelerating the oxidation of UO_2, small quantities of NO_2 can apparently cause the oxidation to proceed beyond U_3O_8 to UO_3 [6–8]. Reported values for the density of UO_3 range from 6.67 to 8.54 g cm^{-3}, depending on the method of measurement and the crystallographic form of UO_3 [9]. It should be noted that some forms of UO_3 are difficult to distinguish from U_3O_8 by X-ray diffraction (XRD). Oxidation of U_3O_8 in NO_2 apparently yields the densest form, ε-UO_3, which would not introduce any additional volume change beyond that for

* Corresponding author. Present address: PCS Inc., Allan Division, Allan, Sask., Canada S0K 0C0. Tel.: +1-306 257 3312; fax: +1-306 257 4240.

[1] Present address: Chalk River Laboratories, Chalk River, Ontario, Canada K0J 1J0.

0022-3115/98/$19.00
PII: S0022-3115(98)00036-1

U_3O_8 formation. Production of the less dense forms of UO_3 could result in volume increases as high as 74%, relative to the initial volume of UO_2.

There is evidence that the quantities of nitrogen oxides generated by gamma radiolysis of a limited volume of air are sufficient to accelerate UO_2 oxidation significantly [6]. These findings are not surprising. Nitrogen dioxide is a ''more efficient oxidizing agent than oxygen in the temperature range 100–500°C'' [10]. As long ago as 1949, Katz and Gruen [11] found that the reaction of U_3O_8 with NO_2 at 250–350°C yields UO_3. However, estimates vary widely as to the concentrations of nitrogen oxides likely to be present in a storage vessel [12–14], and their effect on UO_2 oxidation kinetics is difficult to quantify. Here, we describe an attempt to address the latter problem, by specifically measuring the effects of small concentrations (up to 1.0 vol.%) of NO_2 on the two stages of oxidation of UO_2, i.e., to U_3O_7 [2] and U_3O_8.

2. Experimental

Disks of polycrystalline UO_2 were prepared by slicing pellets of unirradiated CANDU fuel with a low-speed diamond saw. Specimens were prepared with different surface finishes for experiments focusing on the two stages of oxidation. The formation of U_3O_7 proceeds by a diffusion-controlled uniform layer-thickening mechanism, which is best studied on a highly polished surface [15,16]. Therefore, specimens of UO_2 were polished with successively finer media, concluding with 0.05-μm particle-size alumina, in order to examine the effect of NO_2 on the rate of U_3O_7 formation. The formation of U_3O_8, in contrast, proceeds by a nucleation-and-growth mechanism. Previous experience has shown that this occurs most reproducibly on relatively rough surfaces [17–19]. Therefore, some UO_2 specimens were prepared with a 400-grit finish to examine the effect of NO_2 on the rate of U_3O_8 formation.

Compressed, non-standard gas mixtures (air plus 0.1, 0.5, and 1.0 vol.% NO_2) were supplied by Canadian Liquid Air. Specimens were oxidized in a slow-flowing stream ($\sim$ 5 ml min^{-1}) of the air/NO_2 mixtures, or in flowing air, in a small (200 cm^3), vented glass cell mounted inside a Ney Vulcan 3-130 oven, as shown schematically in Fig. 1. The temperature of the oven at the UO_2 sample location (on the floor of the cell) was calibrated relative to the location of the built-in (control) thermocouple, and corrected temperatures are reported herein. Actual temperatures were up to 6°C lower than the nominal set-point value. Experimental temperatures (nominally 225–275°C) and durations ($\sim$ 1–60 h) were selected on the basis of previous experience to yield enough of the target oxidation products to be analyzed by XRD, with complementary surface analysis by X-ray photoelectron spectroscopy (XPS). A few low-temperature (e.g., 150°C) short-duration tests were also performed in order to probe the very early stages of oxidation by XPS alone.

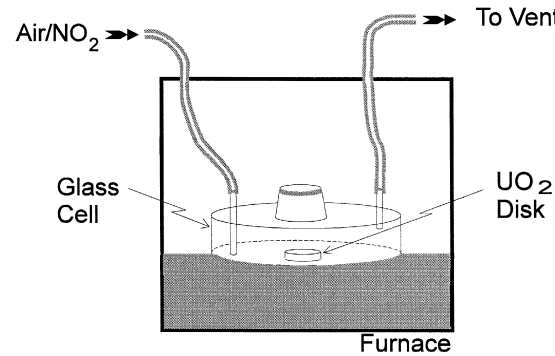

Fig. 1. Illustration of the apparatus used to oxidize UO_2 in the presence of air/NO_2 mixtures.

Selected specimens from many of the U_3O_7 formation tests were examined by X-ray photoelectron spectroscopy, using a PHI-5300 ESCA system, as described elsewhere [20–23]. The XPS spectra were excited using Al-filtered Mg Kα radiation from a source operating at 300 W. The energy scale of the spectrometer was calibrated using the following line positions of noble metals: Au $4f_{7/2}$, 84.0 eV; Ag $3d_{5/2}$, 368.3 eV; and Cu $2p_{3/2}$, 932.56 eV [24–26]. The UO_2 pellet was mounted on an XPS sample holder (PHI Model 190) and out-gassed by pumping for at least 30 min in the side-arm of the spectrometer, before introducing it into the analysis chamber to record its spectra.

Most specimens from the U_3O_7 formation tests, and all of those from the U_3O_8 formation tests, were examined by XRD, using a Rigaku Rotaflex diffractometer equipped with a 12-kW rotating-anode Cu Kα source and a diffracted-beam monochromator. Whenever the same specimen was examined by both XPS and XRD, the XPS work was done first, because this technique is more sensitive to surface contamination, which could potentially occur during transfer and handling.

3. Results and discussion

3.1. Experiments on the kinetics of U_3O_7 formation

3.1.1. X-ray photoelectron spectroscopy

Low-resolution survey spectra were recorded for the 0- to 1100-eV region to determine the elements present in the

[2] The nature of the product of the first stage of UO_2 oxidation varies with the oxidizing conditions and the type of fuel [1]; for example, irradiated light-water reactor fuel forms a cubic U_4O_{9+y} phase rather than tetragonal U_3O_7. Because the experiments described here were performed with unirradiated UO_2 fuel, we refer to the intermediate product as U_3O_7.

sample surface and to check for surface contamination. High-resolution spectra were recorded for the U 4f, O 1s and C 1s regions and the valence bands (0–20 eV), to determine the chemical state of these elements (the carbon signal was due to ubiquitous hydrocarbons present on solid surfaces). The C 1s band was used to correct for charging, by assuming a binding energy value of 284.8 eV for this peak [20,25]. Spectra were recorded at more than one escape angle [24,26] for most of the samples to determine the changes, if any, in the degree of oxidation of the UO_2 samples with surface depth (the XPS sampling depth is a few nanometres).

The band due to the U $4f_{7/2}$ core level is very sensitive to the chemical state of the uranium atoms, and can be quantitatively resolved into U^{6+} and U^{4+} components, as described elsewhere ([22–24,27] and references therein). The relative area of the U^{6+} and U^{4+} peaks is a direct measure of the oxidation state of the uranium atoms in the sample surface. Results obtained from the analysis of the U $4f_{7/2}$ band were verified by analyzing the relative intensities of the bands in the valence region. Table 1 gives a summary of all the XPS results, expressed as both U^{6+}/U^{4+} ratio and % U^{6+}, obtained by analyzing the U $4f_{7/2}$ band. Table 2 lists the expected values of these quantities for various known oxides of uranium.

Table 2
U^{+6}/U^{+4} ratios for various uranium oxides

Formula	U^{+6}/U^{+4} ratio	% U^{+6}
UO_2	0.0	0.0
U_4O_9	0.33	25.0
U_3O_7	0.5	33.3
U_2O_5	1.0	50.0
U_3O_8	2.0	66.7
UO_3	∞	100.0

The U^{6+}/U^{4+} ratio for freshly polished samples, using the procedure described in Section 2, indicates slight oxidation of the UO_2 surface. The observed values of around 0.3 are significantly higher than those typically observed (≤ 0.05) for pellets subjected to a brief, vigorous polishing procedure used in our previous studies [20,22,23]. This suggests that the prolonged, fine polishing procedure used in the present study leads to some surface oxidation of UO_2. We believe that this increased oxidation seen after

Table 1
XPS results on UO_2 oxidation from the analysis of U $4f_{7/2}$ band

Sample number	NO_2 mol%	Conditions		U^{6+}/U^{4+} ratio			% U^{6+}		
		Time (h)	Temp. (°C)	Escape angle			Escape angle		
				25°	45°	65°	25°	45°	65°
1	[a]				0.48	0.45		32.3	31.1
1a	[a]			0.38	0.32	0.15	27.5	24.2	13.0
S1	[a]				0.38			27.5	
S2	[b]				0.05			4.5	
2	0.0	5	269		0.84	0.56		45.7	35.7
2b	0.0	15	269	0.86	0.47	0.33	46.2	32.0	24.8
3	0.1	5	269		6.7	2.6		87.0	71.8
4	0.5	5	269		191	220		99.5	99.5
5	1.0	5	269		13	4.5		92.9	81.7
6	0.0	15	245		1.41	0.56		58.5	35.7
7	0.1	15	245		5.0	4.81		83.3	82.8
8	0.5	15	245		11.3	5.79		91.8	85.3
9	1.0	15	245		21.8	7.38		95.6	88.1
10	0.0	15	224		0.98	0.56		49.4	35.8
11	0.1	15	224		4.4	2.7		81.5	72.8
12	0.5	15	224		6.7	2.4		87.0	70.6
13	1.0	15	224		1.30	0.77		56.5	43.5
13a	1.0	15	224	2.55	1.78	1.34	71.8	64.0	57.3
14	0.0	15	200		0.64	0.45		39.2	31.2
15	0.1	16.5	200		2.2	0.76		68.8	43.3
16	0.5	15	200		3.4	1.3		77.0	56.5
17	1.0	15	200		4.8	1.24		82.8	55.4
18	0.0	4	150		0.99			49.7	
19	1.0	4	150		1.23			55.2	

[a] Freshly polished UO_2.
[b] Prepared by extensive rough polishing (600-grit), using the method described in Refs. [22,23].

'fine polishing' is a result of the longer polishing time (i.e., longer exposure to air), along with local surface heating and perhaps also an increase in the surface reactivity of the UO_2 sample. The decrease in the U^{6+}/U^{4+} ratio with increasing photoelectron escape angles (Table 1) indicates that this oxidation is limited to the outermost few molecular layers, and is therefore well below the detection limit for XRD analysis. Fig. 2 compares the XPS spectrum for the U 4f region of a finely polished UO_2 surface, prepared during this study (sample 1a), with that of a UO_2 surface subjected to brief polishing with a 600-grit SiC abrasive paper (i.e., the method described in Refs. [22,23]). Fig. 3 compares the analyses of the U $4f_{7/2}$ bands of these two samples. The three smooth curves overlaid on each spectrum represent the calculated U^{6+} and U^{4+} components (centred at about 381.1 eV and 379.8 eV, respectively) and their sum. Note the much larger U^{6+} component observed for the highly polished specimen.

The data in Table 1 show that the presence of NO_2 in air increased the average surface oxidation state of uranium in UO_2 specimens at all oxidation temperatures used in the present study. Fig. 4 compares the analyses of the U $4f_{7/2}$ bands of two UO_2 samples subjected to oxidation in air alone, and in air containing 1% NO_2; note the much larger U^{6+} component of the spectrum in the latter case. At temperatures ≥ 200°C, the presence of NO_2 in air leads to the formation of a thin layer of oxide with a U^{6+}/U^{4+} ratio greater than 2, i.e., a surface composition beyond U_3O_8 and approaching UO_3 (Table 2). This highly oxidized layer is very thin, as indicated by the generally lower values of the U^{6+}/U^{4+} ratio at higher escape angles. The one exception is specimen 4 (5 h at 269°C

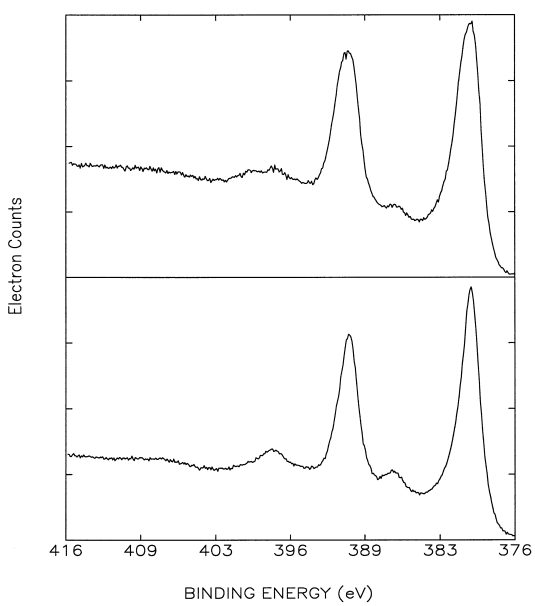

Fig. 2. XPS Spectra for the U 4f Region of UO_2 disks prior to oxidation. (Upper) Highly polished specimen, as described in Section 2 (sample 1a of Table 1). (Lower) Specimen subjected to brief, vigorous polishing with 600-grit SiC abrasive paper as described in Refs. [22,23] (sample S2 of Table 1).

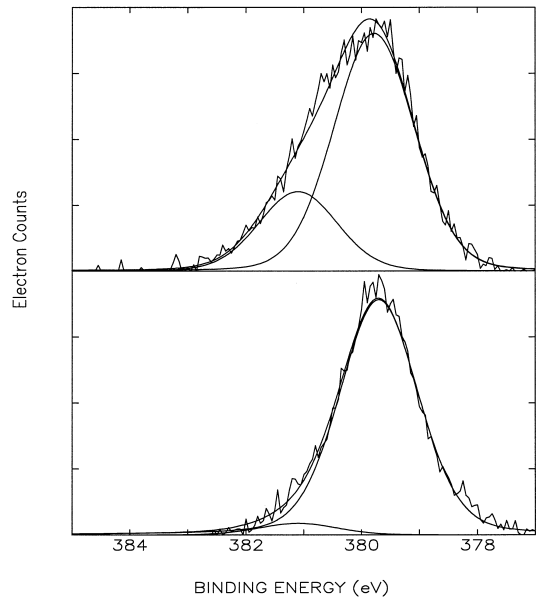

Fig. 3. Analyses of U $4f_{7/2}$ bands in the XPS spectra of UO_2 disks prior to oxidation. (Upper) Highly polished specimen, as described in Section 2 (sample 1a of Table 1). (Lower) Specimen subjected to brief, vigorous polishing with 600-grit SiC abrasive paper as described in Refs. [22,23] (sample S2 of Table 1).

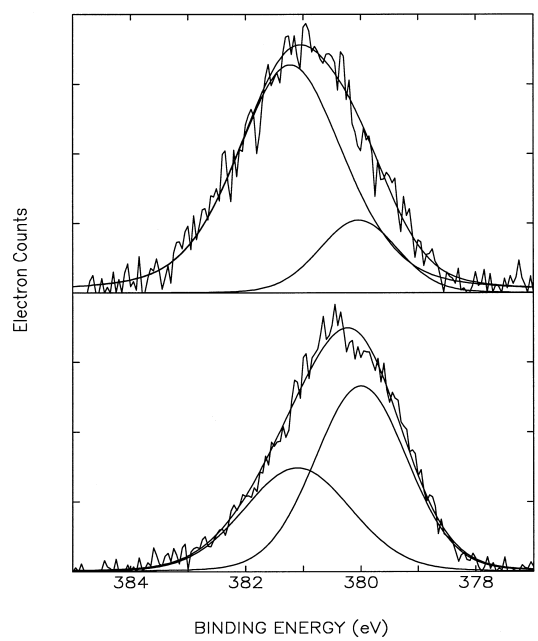

Fig. 4. Analyses of U $4f_{7/2}$ bands in the XPS spectra of UO_2 disks heated at 200°C for 15 h in: (upper) air + 1% NO_2 (sample 17 of Table 1); (lower) air alone (sample 14 of Table 1).

with 0.5% NO_2), which is essentially fully oxidized (> 99% U^{6+}) within the depth accessible to analysis by XPS.

We did not attempt to determine a depth profile of the U^{6+}/U^{4+} ratio near a specimen surface, because ion-milling (sputtering) causes rapid reduction of U^{6+} back to U^{4+}. Although we are thus unable to give a more detailed description of the changes in the surface composition during oxidation, it is quite clear from the data given in Table 1 that the UO_2 samples experienced increased oxidation in the presence of NO_2.

As noted above, several researchers have reported that NO_2 is capable of oxidizing lower oxides of uranium to UO_3. Presumably, when the NO_2 is present at low concentrations and moderate temperatures, formation of UO_3 is limited to a surface film, below which a thicker layer of intermediate oxides can form by diffusion of oxygen into the underlying UO_2 crystal structure. This process is similar to the normal mechanism of air oxidation ([1] and references therein). Oxidation reactions with NO_2 commonly involve its reduction to NO [10,11]. The surface reaction of UO_2 with NO_2 can be represented by reaction (1) or the simplified mechanistic expression (2):

$$UO_2 + NO_2 \rightarrow UO_3 + NO \quad (1)$$

$$U^{4+}(\text{surface}) + NO_2(\text{adsorbed}) \rightarrow U^{6+}(\text{surface}) + O^{2-}(\text{surface}) + NO(\text{gas}). \quad (2)$$

It is well known that NO is rapidly converted to NO_2 by oxygen, even at low temperatures (Eq. (3)):

$$2NO + O_2 \rightarrow 2NO_2. \quad (3)$$

Thus, small quantities of NO_2 probably catalyse the reaction of oxygen with UO_2, rather than acting independently as an additional strong oxidant.

3.1.2. X-ray powder diffractometry

Previous work has shown that XRD can be used successfully for the study of surface oxidation of UO_2, when the oxidized layer is between 0.1 and 2.0 μm thick [15,28]. The XRD patterns of the samples oxidized in this study generally showed progressive oxidation of UO_2 to β-U_3O_7 (or a similar phase), much as described in Ref. [15]. A representative XRD pattern is shown in Fig. 5a. The thickness of the surface layer of U_3O_7 was determined by measuring the integrated intensity $I(UO_2)$ of the [200] diffraction maximum of UO_2 ($d = 0.2735$ nm, $2\theta = 32.72°$) relative to the intensity, $I(U_3O_7)$ of the [002] peak for U_3O_7 ($d = 0.2689$ nm, $2\theta = 33.29°$). The [200] diffraction maximum of U_3O_7 ($d = 0.2773$ nm, $2\theta = 32.26°$) was negligible, because it was greatly diminished by preferred orientation. This phenomenon, and similar effects on other U_3O_7 peaks, has been discussed elsewhere [15]. The XRD peaks used in the present analysis were chosen because they showed the best resolution of U_3O_7 from the UO_2 substrate. Also, being relatively low-angle features, they provide a sensitive measure of layer thickness in the convenient range from 0.1 to 0.5 μm.

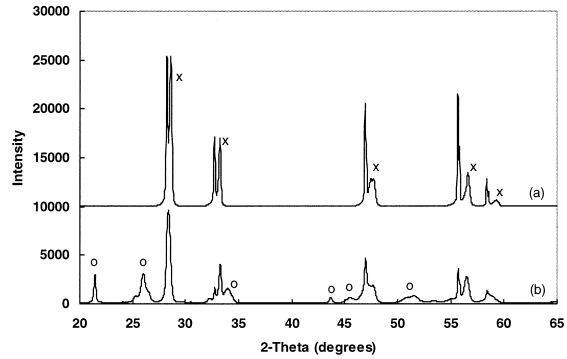

Fig. 5. Representative X-ray diffraction patterns of UO_2 specimens oxidized in air + 0.1% NO_2: (a) at 269°C for 2 h, showing typical U_3O_7 features (x); (b) at 275°C for 6 h, showing typical broad features associated with U_3O_8 or UO_3 (o).

The thickness, τ, of the U_3O_7 layer on the oxidized specimens was calculated using the approximation (Eq. (4)) derived from Ref. [15], where θ is the Bragg angle of the XRD peak and μ is the linear absorption coefficient of U_3O_7 for Cu Kα X-rays, 3.9×10^5 m^{-1}:

$$\frac{I(U_3O_7)}{[I(UO_2) + I(U_3O_7)]} \approx 1 - \exp(-2\mu\tau \operatorname{cosec}\theta). \quad (4)$$

The calculated U_3O_7 layer thicknesses, arranged by oxidation time, temperature and atmosphere, are presented in Table 3 and representative plots are shown in Figs. 6

Table 3
Calculated thicknesses of U_3O_7 layers formed on UO_2 specimens oxidized in air or in air/NO_2 mixtures

Temp. (°C)	Time (h)	U_3O_7 layer thickness (μm)			
		Air	0.1% NO_2	0.5% NO_2	1% NO_2
224	3	0.096	0.139	0.198	0.247
	6	0.147	0.203	0.297	0.375
	9	0.187	0.249	0.339	0.433
	12	0.217	0.270	0.392	0.456
	15	0.240	0.298	0.421	0.482
245	1	–	0.075	0.219	0.163
	2	–	0.141	0.273	0.198
	3	0.245	0.261	0.436	0.291
	6	0.303	0.288	0.486	0.429
	9	0.337	0.340	–	0.480
	12	0.375	0.381	–	0.503
	15	0.430	0.431	–	0.551
269	1	0.131	0.226	0.258	0.329
	2	0.215	0.275	0.329	0.378
	3	0.254	0.319	0.402	0.414
	4	0.317	0.345	0.384	0.438
	5	0.335	0.373	0.429	0.465

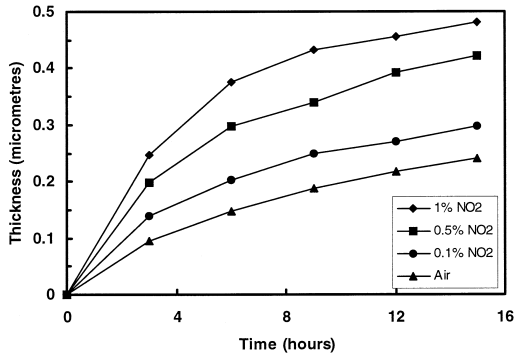

Fig. 6. Thickness of U_3O_7 layer formed on UO_2 disks heated in flowing air or air/NO_2 mixtures for various periods of time at 224°C.

and 7. The data indicate two stages in the U_3O_7 growth kinetics: parabolic up to a thickness of about 0.3 μm, and linear beyond. This is consistent with several reports cited in Ref. [1]. The parabolic stage dominates in the 224°C data (Fig. 6), and the linear stage is predominant in the 269°C data (Fig. 7).

The parabolic reaction kinetics can be fitted to Eq. (5):

$$\tau = (kt)^{1/2}, \tag{5}$$

where t (s) is the time and k (m^2 s^{-1}) is the empirically determined parabolic rate constant. The initial stage of the oxidation reaction was parabolic (Figs. 6 and 7), so the value of k was calculated, for each temperature and concentration of NO_2, by a least-squares fit of the first two data points (plus the origin) to Eq. (5). The resulting rate constants are presented in Table 4. In a few cases (air + NO_2 at 269°C), where reaction rapidly reached the linear-kinetics stage, this procedure tends to underestimate k; this is indicated in Table 4 by presenting the k values as upper limits.

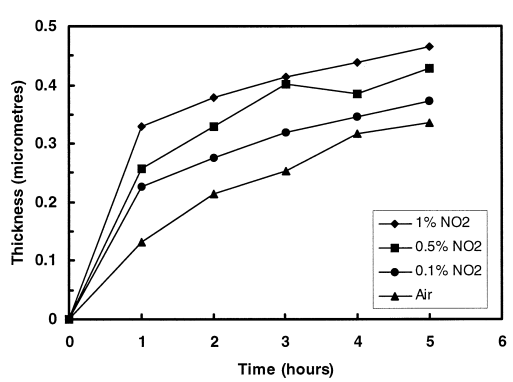

Fig. 7. Thickness of U_3O_7 layer formed on UO_2 disks heated in flowing air or air/NO_2 mixtures for various periods of time at 269°C.

The linear portion of the reaction kinetics was fitted to Eq. (6):

$$\tau = k't, \tag{6}$$

where the linear rate constant k' (m s^{-1}) was determined by linear regression of the last three data points in the reaction curve (e.g., Figs. 6 and 7). The rate constants thus calculated are presented in Table 4. In the case of some of the data for 224°C, the experiment was terminated before the reaction had clearly switched to linear kinetics; the corresponding linear rate constants presented in Table 4 are given as upper limits only.

Examination of the results summarized in Table 4 reveals that the parabolic stage of U_3O_7 growth is dependent on NO_2 concentration, but the linear stage is not. The parabolic stage is consistent with rate-control by chemical diffusion of oxygen through the product layer. This diffusion appears to be accelerated by the formation of an outermost film of highly oxidized material in the presence of NO_2 (see Section 3.1.1). The presence of 1% NO_2 enhances the rate of the diffusion-controlled U_3O_7 formation reaction by about a factor of 2 to 4.

In contrast to the parabolic kinetics, the rate of the linear stage of U_3O_7 layer growth appears to be independent of NO_2 concentration (Table 4), at least at the low concentrations studied herein. McEachern and Taylor [1] concluded that this stage is ''a multifarious process involving cracking and both grain-boundary and intragranular oxidation''. We suggest that the linear kinetic stage observed in the present study is the result of relatively rapid transport of both O_2 and NO_2 through a microcracked outer region, followed by diffusion-controlled oxygen transport through an intact, inner region approximately 0.3 μm in thickness. The rate of U_3O_7 formation is thus limited by the rate of cracking (which allows rapid transport of oxidants to the interior of the sample) which is not dependent on the concentration of NO_2 in the oxidizing atmosphere.

We recognize that the calculated values of k and k' would be improved if more data were available for each combination of temperature and atmosphere. However, experimental limitations, in particular the need to cool and remove specimens for XRD, restricted the frequency of sampling and analysis.

3.2. Experiments on the kinetics of U_3O_8 formation

We have fewer data to report for the second step of oxidation (to U_3O_8) than for the first step (to U_3O_7). The number of experiments was limited by time, and by the availability of specialty gas mixtures. Specifically, the experiments required flowing air/NO_2 mixtures, which would be difficult to maintain for the very long reaction times (weeks near 250°C; months near 200°C; years near 150°C) required to measure U_3O_8 formation by XRD at lower temperatures [1,17,19,22,23]. Moreover, since our

Table 4
Parabolic (k) and linear (k') rate constants for the formation of U_3O_7 on the surface of UO_2 in air and air/NO_2 mixtures

Model	Temp (°C)	Rate constant[a]			
		Air	0.1% NO_2	0.5% NO_2	1.0% NO_2
Parabolic	224	9.47×10^{-19}	1.87×10^{-18}	3.93×10^{-18}	6.25×10^{-18}
	245	4.69×10^{-18}	2.32×10^{-18}	1.13×10^{-17}	6.08×10^{-18}
	269	5.84×10^{-18}	$<1.17\times10^{-17}$	$<1.61\times10^{-17}$	$<2.30\times10^{-17}$
Linear	224	$<2.45\times10^{-12}$	$<2.27\times10^{-12}$	$<3.81\times10^{-12}$	2.27×10^{-12}
	245	3.06×10^{-12}	4.22×10^{-12}	4.64×10^{-12}	3.28×10^{-12}
	269	1.13×10^{-11}	7.50×10^{-12}	3.75×10^{-12}	7.08×10^{-12}

[a]The parabolic rate constant, k, is in units of $m^2\ s^{-1}$; the linear rate constant, k', is in units of $m\ s^{-1}$.

main concern is the effect of NO_2 on oxidation at temperatures below 200°C, there was little to gain from examining the reaction at temperatures in excess of 300°C. Thus, the effect of NO_2 on the rate of U_3O_8 formation was examined only at 275°C.

Table 5
Kinetic parameters F and κ for UO_2 surfaces oxidized to U_3O_8 at 275°C in air and air/NO_2 mixtures

[NO_2] (%)	Time (h)	F	κ (h^{-3})
0.0	7	0	3.2×10^{-5}
	15	0.348	
	23	0.414	
	31	0.487	
0.0	17.6	0.315	3.9×10^{-5}
	25.6	0.417	
	33.6	0.472	
0.0	8	0.155	1.8×10^{-4}
	16	0.499	
0.0	4	0	5.5×10^{-5}
	24	0.536	
0.0	8	0.065	8.1×10^{-5}
	18	0.381	
0.1	6	0.765	6.8×10^{-3}
0.1	6	0.516	3.3×10^{-3}
0.5	2	0.000	1.6×10^{-3}
	4	0.259	
	6	0.239	
0.5	6	0.000	9.6×10^{-4}
	12	0.914	
1.0	6	0.000	9.2×10^{-4}
	12	0.892	
1.0	6	0.877	1.0×10^{-2}
1.0	2	0.000	1.5×10^{-3}
	4	0.036	
	6	0.278	

Values for 0.0% NO_2 are taken from Table 2 of Ref. [19], where they are listed as $\alpha(t)$.
F is the fraction of the sample surface oxidized to U_3O_8 within the XRD sampling depth (1–2 μm).
The rate constant κ is a composite for both the nucleation and growth of U_3O_8 defined by Eq. (7) and described by McEachern et al. [19].

After oxidation in air or air/NO_2, the samples were cooled to room temperature, and the XRD spectra were recorded. The XRD data were used to estimate the fraction, F, of UO_2 converted to U_3O_8 within the outermost 1–2 μm analyzed by XRD, following the procedure described by Choi et al. [18]. Calculated values of F as a function of time, temperature, and oxidizing atmosphere are summarized in Table 5.

It has been shown recently [19] that the formation of U_3O_8 on the surface of a UO_2 specimen can be represented by the following kinetic expression for two-dimensional nucleation and growth:

$$F = 1 - \exp\left\{-\frac{\pi\kappa t^3}{3} + \frac{\pi^2\kappa^2 t^6}{180} - \frac{11\pi^3\kappa^3 t^9}{45\,360} + \frac{5\pi^4\kappa^4 t^{12}}{399\,168}\right\}, \quad (7)$$

where F is the fraction of the surface oxidized to U_3O_8, t is time, and κ is a composite rate constant that incorporates the rates of both nucleation and growth of U_3O_8. The kinetic data on the rate of U_3O_8 formation were fitted to Eq. (7) by varying the value of κ to minimize the sum of the squares of deviations between experimental and calculated values of F. The resulting calculated values of κ are presented in Table 5. The variation in κ as a function of NO_2 concentration is illustrated in Fig. 8.

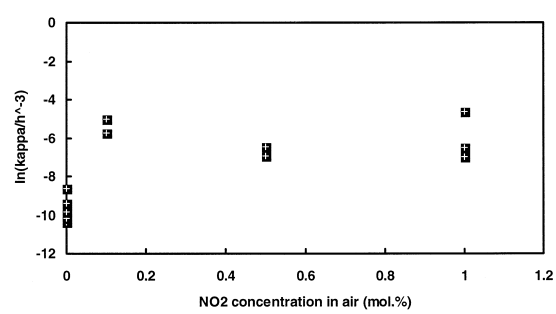

Fig. 8. Variation in the composite rate constant, κ, for U_3O_8 formation, as a function of NO_2 concentration of the oxidizing atmosphere at 275°C.

Examination of Fig. 8 reveals that the presence of NO_2 in the oxidizing atmosphere results in a striking increase in the rate of formation of U_3O_8. The rate constant κ is about two orders of magnitude greater in the presence of NO_2 than in air at 275°C. Moreover, there does not appear to be any correlation between κ and the concentration of NO_2 in the range 0.1 to 1.0 vol.%. These results raise the possibility that even small quantities of radiolytically generated NO_2 may increase the rate of U_3O_8 growth on the oxidized surfaces of UO_2 fuel fragments by a substantial amount. It must be noted, however, that an increase in the rate constant, κ, by two orders of magnitude does not increase the rate of formation of U_3O_8 by two orders of magnitude. The complex nature of Eq. (7) does not lead to a simple linear relationship between κ and the rate of U_3O_8 formation; rather, an increase in κ by *three* orders of magnitude results in an increase in the rate of formation of U_3O_8 by approximately *one* order of magnitude.

The results reported herein on the impact of NO_2 on the oxidation of unirradiated UO_2 are supported by recent work described by Sunder and Miller [22,23]. The value of the composite U_3O_8 formation rate constant for air oxidation at 150°C has been estimated as 1.67×10^{-17} h^{-3} by McEachern et al. [19]. This value of κ corresponds to a value of F of 0.109 after 21.5 years. In contrast, Sunder and Miller [22,23] found that UO_2 disks placed in sealed ampoules (air atmosphere) at 150°C in a gamma field of ≈ 15 Gy h^{-1} displayed an average value of $F = 0.109$ [3] after 1.84 years. Thus, the rate of U_3O_8 production in the Sunder and Miller experiments [22,23] is approximately one order of magnitude greater than the results calculated by McEachern et al. [19]. We believe that this is due to the presence of radiolytically generated NO_2 in the former experiments.

Disks of UO_2 that have undergone air oxidation to F values greater than 0.5 generally display U_3O_8 powder formation and spalling [18,19]. However, visual observation of the disks oxidized under NO_2 atmospheres at 275°C did not reveal any evidence for powder formation or spalling, even though many of them had a high degree of surface oxidation (Table 5). It thus appears that the presence of NO_2 may alter the morphology of the U_3O_8, making it less prone to spalling. Alternatively, surface oxidation may have gone beyond U_3O_8 to UO_3 (Section 3.1.1). It was not possible to determine, from the XRD patterns, whether the surface (1–2 μm) oxidation was to U_3O_8 or UO_3 because several of the reported U_3O_8 and UO_3 oxidation patterns are very similar [29]. The peaks in the XRD patterns of the ultimate oxidation product in air/NO_2 are too broad (because of small crystallite size) to distinguish among such patterns. This point is illustrated by a representative XRD pattern in Fig. 5b.

[3] Average value of the three samples L, P and Q described in Table 3 of Ref. [23].

4. Conclusions

Oxidation of UO_2 disks in air or air/NO_2 atmospheres at 224 to 269°C initially displayed formation of U_3O_7 by parabolic kinetics, but then switched to linear kinetics after the formation of an oxide layer ca. 0.3 μm thick. The parabolic rate constant increased with the concentration of NO_2, but the effect is not dramatic; in the presence of 1% NO_2, the rate of formation of U_3O_7 is 2–3 times faster than in the presence of air. In contrast to the case of parabolic kinetics, the formation of U_3O_7 in the linear-kinetic region appears to be independent of the concentration of NO_2.

Examination of the surface of UO_2 disks oxidized under air/NO_2 atmospheres by XPS revealed a thin film of highly oxidized material with a composition beyond U_3O_8 and approaching UO_3. The high oxygen potential of this film may be responsible for the accelerated formation of U_3O_7 in the parabolic (diffusion-controlled) kinetic regime.

The effect of NO_2 on the rate of formation of U_3O_8 is more dramatic than on U_3O_7 formation, but it is also more difficult to study, because of the long reaction times and high variability in the extent of the oxidation reaction. Our preliminary data obtained at 275°C suggest that the presence of NO_2 in dry air may increase the composite nucleation-and-growth rate constant, κ, for U_3O_8 formation by about two orders of magnitude, even for low concentrations of NO_2. The corresponding increase in the rate of production of U_3O_8 is close to an order of magnitude. Thus, radiolytically generated NO_2 might accelerate the formation of U_3O_8 on defective elements of used (irradiated) fuel under nominally dry air storage conditions. This would at least partly offset the increased resistance of used fuel, as compared with unirradiated UO_2, to U_3O_8 formation [1,18].

Acknowledgements

The authors appreciate critical review of this document by L.H. Johnson and J.C. Tait. This work was funded by AECL through the Underlying Chemistry research program.

References

[1] R.J. McEachern, P. Taylor, 254 (1998) 87. 281-I (1997).
[2] D.G. Boase, T.T. Vandergraaf, Nucl. Technol. 32 (1977) 60.
[3] R.E. Einziger, J.A. Cook, Nucl. Technol. 69 (1985) 55.
[4] J. Novak, I.J. Hastings, E. Mizzan, R.J. Chenier, Nucl. Technol. 63 (1983) 254.

[5] J.S. Anderson, L.E.J. Roberts, E.A. Harper, J. Chem. Soc., (1955) 3946.
[6] T.K. Campbell, E.R. Gilbert, G.D. White, G.F. Piepel, B.J. Wrona, Nucl. Technol. 85 (1989) 160.
[7] E.R. Gilbert, G.D. White, C.A. Knox, Proc. of International Workshop on Irradiated Fuel Storage: Operating Experience and Development, held in Toronto, ON, 1984, p. 551.
[8] G.D. White, C.A. Knox, E.R. Gilbert, A.B. Johnson, Jr., Proc. of NRC Workshop on Spent Fuel/Cladding Reaction During Dry Storage, held in Gaithersburg, MD, NUREG/CP-0049, 1983, p. 102.
[9] H.R. Hoekstra, S. Siegel, J. Inorg. Nucl. Chem. 18 (1961) 154.
[10] I.R. Beattie, in: A.A. Eldridge et al. (Eds.), Mellor's Comprehensive Treatise on Inorganic and Theoretical Chemistry, Vol. VIII, Suppl. II, Sec. XXVII. Longmans, Green, London, 1967.
[11] J.J. Katz, D.M. Gruen, J. Am. Chem. Soc. 71 (1949) 2106.
[12] A.H. Spellar, E.O. Maxwell, R.J. Pearce, Proc. of B.N.E.S. Conference on Gas Cooled Reactors Today, Vol. 4, held in Bristol, UK, 1982, p. 25.
[13] A.B. Johnson, Jr., E.R. Gilbert, D.R. Oden, D.L. Stidham, J.E. Garnier, D.L. Weeks, J.C. Dobbins, Proc. Waste Management '85, Vol. 1, Tucson, AZ, 1985, p. 513.
[14] K.M. Wasywich, C.R. Frost, Proc. of 3rd Intl. Conf. on High Level Radioactive Waste Management, Las Vegas, 1992, p. 1166.
[15] P. Taylor, E.A. Burgess, D.G. Owen, J. Nucl. Mater. 88 (1980) 153.
[16] P. Taylor, D.D. Wood, A.M. Duclos, J. Nucl. Mater. 189 (1992) 116.
[17] R. McEachern, J. Nucl. Mater. 245 (1997) 238.
[18] J.-W. Choi, R.J. McEachern, P. Taylor, D.D. Wood, J. Nucl. Mater. 230 (1996) 250.
[19] R.J. McEachern, J.-W. Choi, M. Kolar, W. Long, P. Taylor, D.D. Wood, J. Nucl. Mater. 249 (1997) 58.
[20] S. Sunder, G.D. Boyer, N.H. Miller, J. Nucl. Mater. 175 (1990) 163.
[21] S. Sunder, J.J. Cramer, N.H. Miller, Mater. Res. Soc. Symp. Proc. 257 (1992) 449.
[22] S. Sunder, N.H. Miller, J. Nucl. Mater. 231 (1996) 121.
[23] S. Sunder, N.H. Miller, Report, AECL-11351, COG-95-296 (1995).
[24] C.D. Wagner, W.M. Riggs, L.E. Davis, J.F. Moulder, G.E. Muilenberg, Handbook of X-ray Photoelectron Spectroscopy, Perkin-Elmer, Eden Prairie, MN, 1979.
[25] N.S. McIntyre, S. Sunder, D.W. Shoesmith, F.W. Stanchell, J. Vac. Sci. Technol. 18 (1981) 714.
[26] D. Briggs, M.P. Seah (Eds.), Practical Surface Analysis by Auger and X-Ray Photoelectron Spectroscopy, Wiley, Chichester, UK, 1983.
[27] S. Sunder, D.W. Shoesmith, M.G. Bailey, F.W. Stanchell, N.S. McIntyre, J. Electroanal. Chem. 130 (1981) 163.
[28] P.A. Tempest, P.M. Tucker, J.W. Tyler, J. Nucl. Mater. 151 (1988) 251.
[29] L.E. Thomas, R.W. Knoll, L.A. Charlot, J.E. Coleman, E.R. Gilbert, Report, PNL 6640 (1989).